Role of Metal Contacts on Halide Perovskite Memristors

José Carlos Pérez-Martínez, Mariana Berruet, Cedric Gonzales, Saeed Salehpour, Ali Bahari, Belén Arredondo, and Antonio Guerrero*

Halide perovskites are promising candidates for resistive memories (memristors) due to their mixed electronic/ionic conductivity and the real activation mechanism is currently under debate. In order to unveil the role of the metal contact and its connection with the activation process, four model systems are screened on halide perovskite memristors: Nearly inert metals (Au and Pt), low reactivity contacts (Cu), highly reactive contact (Ag and Al), and pre-oxidized metal in the form of AgI. It is revealed that the threshold voltage for activation of the memory effect is highly connected with the electrochemical activity of the metals. Redox/capacitive peaks are observed for reactive metals at positive potentials and charged ions are formed that can follow the electrical field. Activation proceeds by formation of conductive filaments, either by the direct migration of the charged metals or by an increase in the concentration of halide vacancies generated by this electrochemical reaction. Importantly, the use of pre-oxidized Ag^+ ions leads to very low threshold voltages of ≈0.2 V indicating that an additional electrochemical reaction is not needed in this system to activate the memristor. Overall, the effect of the metal contact is clarified, and it is revealed that AgI is a very promising interfacial layer for low-energy applications.

J. C. Pérez-Martínez, M. Berruet, C. Gonzales, S. Salehpour, A. Guerrero
Institute of Advanced Materials (INAM)
Universitat Jaume I
Castelló 12006, Spain
E-mail: aguerrer@uji.es
J. C. Pérez-Martínez
Electronic Technology Area
Universidad Rey Juan Carlos
Móstoles 28933, Spain
M. Berruet, B. Arredondo
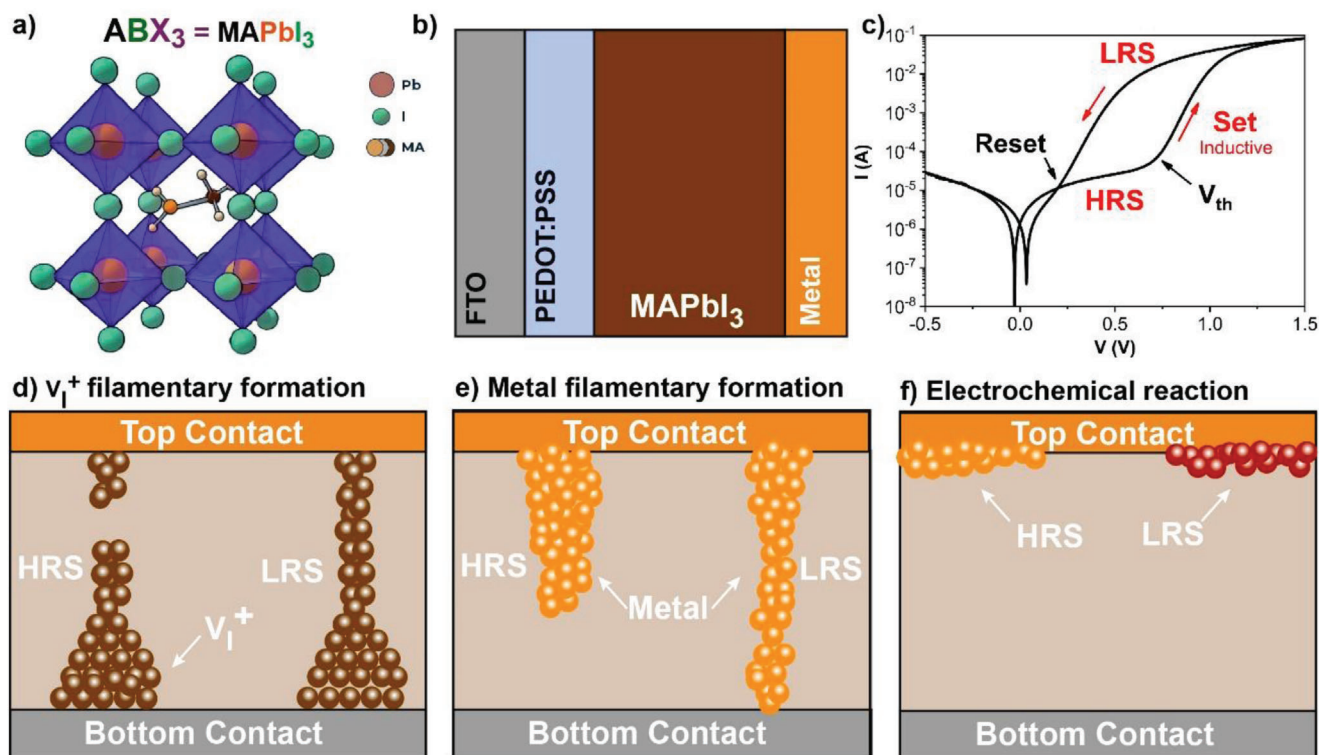División Electroquímica Aplicada
INTEMA
CONICET-Universidad Nacional de Mar del Plata
Mar del Plata B7606BWV, Argentina
S. Salehpour, A. Bahari
Department of Physics
Faculty of Basic Sciences
University of Mazandaran
Babolsar 4741695447, Iran

1. Introduction

Halide perovskites are a family of materials initially developed for photovoltaic cells that find applications as memory devices,[1–3] artificial synapses[4] for neuromorphic computation,[5] and photoactive synapses suitable to artificial vision devices.[6] The perovskite materials follow the general formula ABX_3 where A = monovalent cations, B = divalent cation, and X = halide anion[7] as illustrated in **Figure 1a**. The perovskite, as a material platform, possesses a large degree of freedom with a compositional space of >10^6 formulations of mixed cations and anions combinations allowing tailored device design for versatile optoelectronic applications.[8] Halide perovskites have gained considerable attention as an emerging technology for memory applications owing to their mixed ionic-electronic conduction due to halide vacancy (V_X^+) migration (Figure 1a).[9] The V_X^+ migration and redistribution considerably modify the current extraction leading to the intrinsic memory effects (hysteresis) in the current–voltage ($I - V$) curves.[10] Instead of minimizing the hysteresis effect for perovskite solar cells, this intrinsic memory effect is exploited in neuromorphic computing applications as memristor devices.

A memristor is a two-terminal device whose resistance state changes depending on the history of the electric stimuli applied to the device. This memristive response is denoted as resistive switching. The typical perovskite-based memristor configuration and the representative characteristic $I - V$ response are illustrated in Figure 1b,c, respectively. The representative resistive switching involves the transition from a high resistance state (HRS) or OFF state to a low resistance state (LRS) or ON state at a certain threshold voltage (V_{th}) via a voltage sweep in the forward direction promoting the SET process.[11] Notably, in the reverse scan direction of the same polarity, the transition from LRS to HRS (RESET process) occurs at a lower threshold voltage.[12] This is a threshold resistive switching-type memristive response exhibiting volatile memory where the ON state relaxes back to the OFF state upon the removal or sufficient decrease of the applied external voltage.[12] In particular, this memristive response can be considered as a large inverted hysteresis where the current measured in the forward direction is lower than the current measured in the reverse direction (Figure 1c) due to the presence of a chemical inductor.[11c,13]

Figure 1. a) Representative perovskite crystalline structure of MAPbI$_3$. b) Device architecture used in this work, c) Representative $I - V$ curve of a device containing Au at a scan rate of 100 mV s^{-1}, activation, and deactivation mechanism proposed in the literature. d) Conductive filamentary formation of V_I^+, e) Metal filamentary formation, and f) Electrochemical reaction at the interfaces.

Memristive response has been demonstrated in a wide array of perovskite-based memristors with various formulations,[14] configurations with buffer layers,[15] and distinct metal contacts.[16] These efforts have led to rapid progress in perovskite memristor performances that enable their use in different neuromorphic computing schemes.[17] Despite this rapid development of perovskite formulations and configurations as memristor devices exhibiting unique switching physics, the underlying operational mechanisms are yet to be fully elucidated. A recent review highlights the lack of a clear understanding on the resistive switching mechanism as several physical and chemical processes have been reported.[16] Some of these resistive switching mechanisms range from filamentary formation of iodide vacancies (V_I^+) (Figure 1d), filamentary formation of metal contact typically with a more reactive Ag (Figure 1e), and interfacial chemical reaction between migrating ions and Ag contacts (Figure 1f). Other mechanisms have also been proposed, including modification of the internal Schottky barrier, trapping/de-trapping mechanism, or self-doping of the perovskite material.[18] However, even with nearly inert metals, ions have also been observed to migrate through the perovskite layer depending on the external conditions.[19] Providing a clear understanding on the system is a huge task and can only be accomplished by a careful selection of metals encompassing a wide range of electrochemical reactivities. Hence, a more systematic investigation of the typical metals used as top electrodes in perovskite memristors ranging from nearly inert (Au, Pt), low reactivity (Cu), to high reactivity (Ag, Al) metals is essential to provide valuable insight on the resistive switching mechanisms in perovskite memristors. More importantly, the connection of

the selected contact with the electronic response has not been studied to date.

In this work, we fabricate several model methylammonium lead iodide (MAPbI$_3$) memristors with different top electrode metals that are directly in contact with the perovskite layer to account for different chemical reactivity: nearly inert (Au, Pt), low reactivity (Cu), to high reactivity (Ag, Al). We have also included a layer of pre-oxidized Ag$^+$ ions in the form of AgI. The MAPbI$_3$ perovskite formulation is selected as the archetypal material for a simple and well-established understanding of the operational mechanisms. Analysis of the $I - V$ curves and SEM micrographs of devices containing the nearly inert Au or Pt metals reveal the migration of oxidized metal ions toward the perovskite bulk layer promoting the SET process from the HRS to the LRS. On the other hand, capacitive redox peaks associated with the oxidation and reduction reactions in the different polarities are observed. When reactive metals are used, the oxidation of the metal (i.e., Ag(0) to Ag$^+$) may mask the inductive memristive response of the device. Most notably, the scan rate-dependent threshold SET voltages of the memristors with pre-oxidized metal contacts are clearly linked to a lower threshold voltage of the SET process.

2. Results and Discussion

Memristors have been fabricated in the configuration glass/FTO/PEDOT:PSS/MAPbI$_3$/Metal/Au according to previously reported methods described in the supplementary materials, where FTO is Fluorine doped tin oxide and PEDOT:PSS is Poly(3,-4-ethylenedioxythiophene-)poly(styrenesolfonate). The
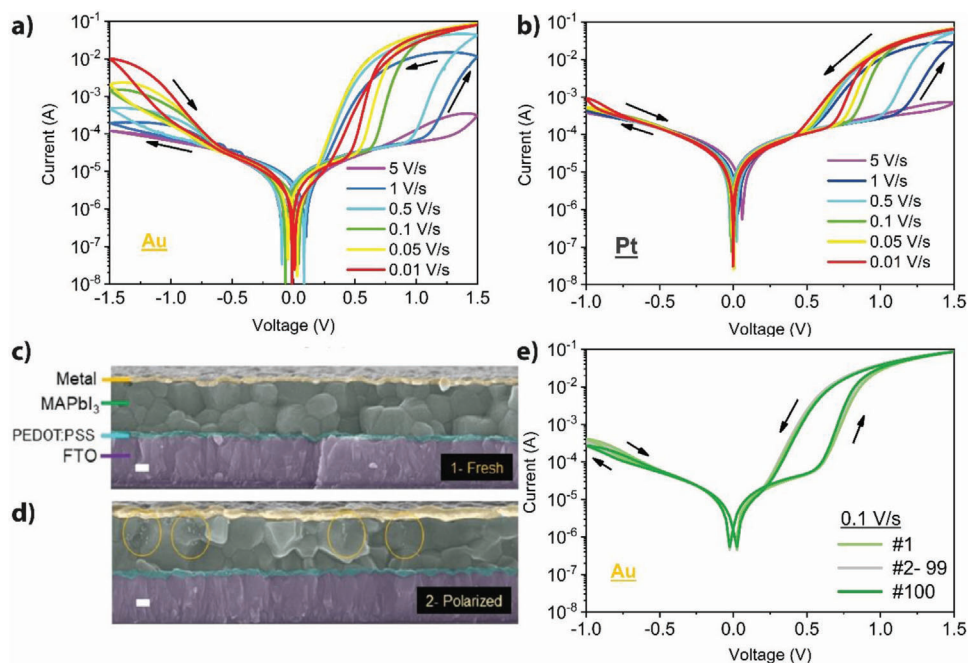
Figure 2. *I–V* curves of devices fabricated with a) Au and b) Pt as a function of the scan rate. Cross-section SEM images of devices containing Au as contact: c) a fresh device and d) A device that has been polarized at positive voltages with a scale bar of 100 nm. e) *I–V* curves of the fresh device shown in (c).

top contact is composed of two layers; the first one contains the metal under study (15 nm) and the second Au layer (60 nm) acts as a current collector. The bottom contact contains PEDOT:PSS that helps to reduce the roughness of the FTO providing a flat surface where the perovskite grows as a continuous layer. In addition, the reactivity of migrating ions with PEDOT:PSS is considered to be low as compared to oxides such as FTO. The top contact is fabricated with a selection of metals that probe different reactivities: Au, Pt, Cu, Ag, Al, and pre-oxidized Ag ions in the form of AgI. In the following sections, we will separate the behavior of relatively inert metals from those more reactive metals.

2.1. Low Reactivity Metals

Gold and platinum are two noble metals that have been used in the solar cell configuration due to the relatively high inertness toward the perovskite material.[20] Here, we fabricated memristors with Au or Pt and the *I–V* responses (**Figure 2**a,b) are very similar showing large variations in the hysteresis as a function of the scan rate, in agreement with previously reported results.[21] We note that the electrical response is reproducible for different devices fabricated within the same batch as shown in the supplementary material (Figure SI1, Supporting Information). The response is mainly inductive at positive bias; with lower current in the forward direction than in the reverse direction. The set voltage (V_{SET}) depends on the scan rate with values in the range from +0.5 to +1.3 V and ON/OFF ratios that approach three orders of magnitude. All these devices show the response of volatile memories where the reset process occurs at positive bias with crossing points at +0.2 to +0.75 V, see the reset crossing point at positive bias in Figure 2e.[16] Results for Pt are very similar with a small

variation in the ON/OFF ratios that is within the dispersion of the results.

Complete devices based on Au have been analyzed by cross-section scanning electron microscopy (SEM) with the aim to identify migrating metal particles to understand if metal migration is one of the main activation mechanisms in this configuration. A representative image of a device that was only subjected to three cyclic voltammetry scans at 0.1 V s⁻¹ (3 min of measurement time) is shown in Figure 2c with the label "fresh", and the *I–V* curve shown in Figure 2e corresponds to the first three cycles of an analogous sample. In many of the presented *I–V* curves the data does not cross the origin, that is, at 0 V the current is not zero. We have discussed this in previous works, and it is closely connected with the presence of the charged ions at the interfaces with the contacts to form a type of double-layer supercapacitor. In this situation, the interfaces with the contacts are charged and the perovskite material acts as a partially electrically insulating membrane.[22]

The SEM image shows high-quality and crystalline perovskite with large domains (100–400 nm) without the presence of metal particles or filaments across the perovskite layer. Alternatively, the *I–V* curve shows that the device immediately turns on during the first scan of the cycling voltammetry without the need of electroforming at higher voltages. The result would be compatible with activation/deactivation of the memory due to halide vacancies (V_I^+) migration as proposed by Gu and co-workers.[23] Alternatively, samples that are measured for more than 100 cycles show large bright metal particles (>10 nm) in the SEM images, see highlighted regions of the polarized sample in Figure 2d. According to the SEM analysis, this result would imply that it is also possible that metal filaments are formed under the presence of an electrical field. Note that very thin Au filaments in the order of nm would be sufficient to act as a percolation

**ADVANCED
SCIENCE NEWS**

www.advancedsciencenews.com

**ADVANCED
FUNCTIONAL
MATERIALS**

www.afm-journal.de

pathway for the charge and would be beyond the resolution of our experiment. Therefore, according to this experiment, the activation mechanism of the memristors is not conclusive as filamentary formations could well be generated by both V_I^+ or metal ions.

2.2. Reactive Metals

In the previous case, if activation/deactivation is due to metal migration it is difficult to explain how "non-reactive" metals evaporated in oxidation state zero may follow the applied electric field. In other words, what would be the driving force for neutral metal particles that have no net charge to follow the external electric field? The simplest response is that Au suffers from a slow oxidation at the interface in the presence of the perovskite. This oxidation can occur spontaneously[21] or it may be electrochemically promoted by applying a positive voltage. Indeed, systems that lead to clear redox/capacitive peaks will be shown in this section and this will help to re-analyze the data from non-reactive metals.

Reactive metals such as Copper, Silver, or Aluminum may be used since they have enough electrochemical capability to react at the interface with the perovskite spontaneously or with a small help of an applied positive voltage. The corrosion behavior of a metal is related to its electrochemical stability, which in turn may be determined by its work function. Thus, reactivity of the metals would be expected to be in the order Au ≈ Pt < Cu < Ag < Al with increasing reactivity as the work function decreases (see supplementary information). A clear example of this favored reactivity is observed in the field of solar cells where AgI formation is known to be the main degradation pathway of cells containing Ag metal as current collector.[25]

The $I–V$ curves of devices fabricated with Cu and Ag are shown in **Figure 3**. The response of Cu reminds very much that of the devices containing Au or Pt with inductive response at fast scan rates of 1 V s^{-1} (Figure 3a). However, at slow scan rates (Figure 3b) a capacitive peak is observed in the range of 0 to +0.8 V that corresponds to oxidation of Cu(0) to Cu(I) or Cu(II). At this point, we remind the reader that capacitive peaks are typically observed in redox reactions and can be identified with a higher current in the forward direction than in the reverse direction.[26] These slow scan rates let the system be in the positive bias during long times to initiate the electrochemical reactions. Similarly, at negative potentials the presence of two capacitive peaks is evident. These peaks should correspond to the complementary reduction reactions from Cu (II)/Cu(I) to Cu(I)/Cu(0) respectively. It is important to note that the precise nature of the electrochemical reactions involved is difficult to analyze and further reactions in the solid state with the perovskite are also possible with formation of vacancies and generation of PbI$_2$. In any case, we highlight that the inductive peak needed for memory devices is masked by the capacitive peak and a clear memory response is not observed at low scan rates. This statement is further confirmed during the course of 100 cycles at scan rates of 0.1 V (Figure 3c) with one of the capacitive peaks disappearing at negative voltages.

Alternatively, when Ag is used as a reactive metal (Figure 3d), a very large capacitive peak is observed at high scan rates of 1 V s^{-1}.

Here, the capacitive current related to formation of oxidized silver is very large and totally masks the inductive response of the memory device. In this case, the metal readily oxidizes even at high scan rates accounting for a more reactive metal and most of the response is capacitive even at negative voltages. On the contrary, the inductive response that leads to the resistive switching is only observed at lower scan rates (i.e., 0.01 V s^{-1}), possibly because at these scan rates most of the interfacial Ag (0) has already reacted within the first mV (100 slower sweep than 1 V s^{-1}). The development of the capacitive peaks at positive and negative bias with the cycling of the device is clearly observed at intermediate scan rates of 0.1 V s^{-1} (Figure 3f). Here, for data completeness, we have included in the supporting information devices containing the highly reactive Al metal.

The difference in scan rates among capacitive and inductive responses with reactive metals could indicate kinetic and transport-limited dynamical current. We note that oxidation and reduction of the metal contacts are the obvious electrochemical semireactions at positive and negative bias, respectively. However, establishing the complementary redox semireaction is very usually challenging for solid-state electrochemical reactions and will not be the subject of this work.[19b] Here we propose that the evaporated Ag (0) present in the fresh device at 0 V oxidizes as a positive voltage bias is applied. An anodic peak appears associated with oxidation of silver (Semireaction I) and a complementary reduction reaction occurs in the perovskite layer. Simultaneously, iodide ions of perovskite diffuse to the interface MAPbI$_3$/metal by electrostatic drift field (positive polarization applied at metallic electrode) giving rise to formation reaction of AgI. As described above, the complementary redox reaction is thought to be connected to the redox couple I$_2$ + 2e$^-$ → 2I$^-$ (Semireaction II) possibly mediated by the perovskite material.[19b] A simple way to visualize this type of complex electrochemical reaction can be described by the coupling of Reactions I and II. This could be taken as a first step toward the overall formation of AgI that is thermodynamically favored. Then, reverse scan direction allows the reduction reaction from Ag$^+$ (I) to Ag (0) at negative bias. In any case, it is important to note that the oxidation of Ag (0) acts as an iodide sink by the formation of AgI, and this involves a loss of iodide ions from the perovskite layer in the form of additional halide vacancies (V_I^+).

$$Ag \rightarrow Ag^+ + e^- \tag{1}$$

$$\frac{1}{2}I_2 + e^- \rightarrow I^- \tag{2}$$

$$Ag^+ + I^- \rightarrow AgI \tag{3}$$

If we now go back to the response of low reactivity metals like Au or Pt and one analyzes carefully the $I–V$ traces in Figure 2a, a capacitive peak is observed at voltages > +0.6 V and scan rates of 0.01 V s^{-1}, see the red trace and the second crossing point. In this particular example, the presence of the capacitive peak would indicate the slow oxidation of Au to Au(I) or Au(III) with formation of Au iodides (AuI and AuI$_3$).[24] Therefore, it is clear that a preconditioning reaction is needed to oxidize the metal so that the metal is charged and thus it is able to migrate following the external electric field. This electrochemical reaction is often referred
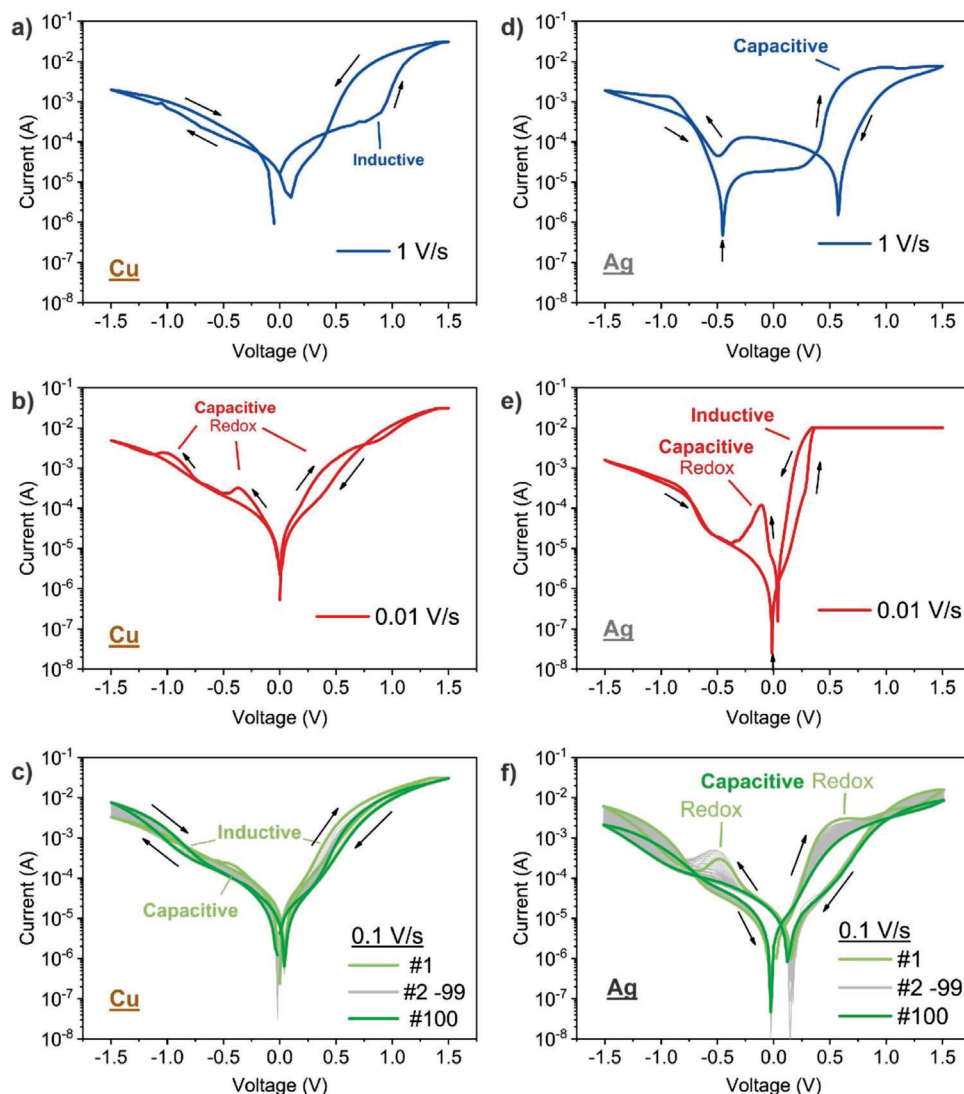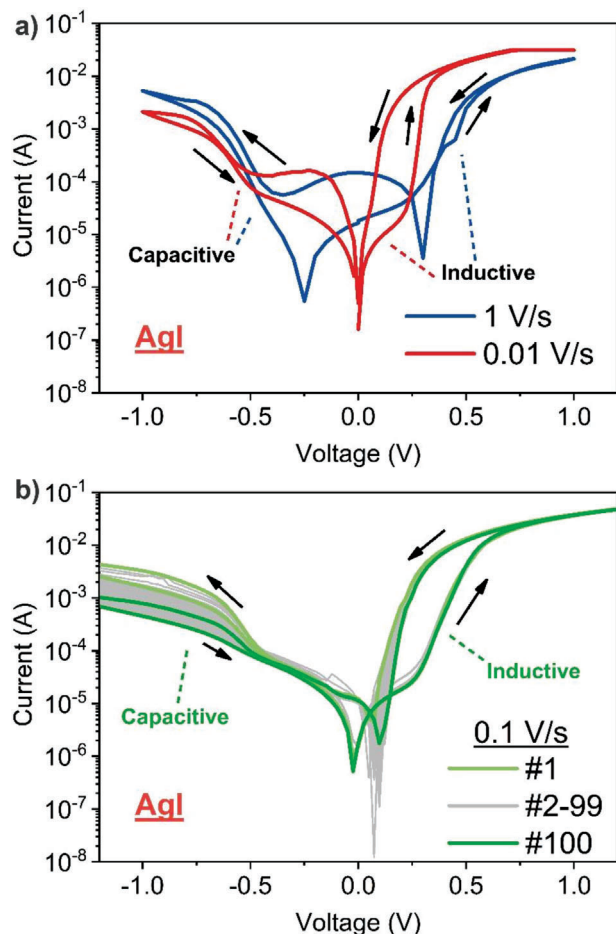
Figure 3. Current–voltage (I–V) sweeps of devices fabricated in the configuration FTO/PEDOT:PSS/MAPbI$_3$/metal/Au devices with a–c) Metal = Cu and d–f) Metal = Ag (a) and (d) have been cycled at fast scan rates, (b) and (e) have been cycled at slow scan rates and (c), and (f) show 100 cycles at a scan rate of 0.1 V s^{-1} for the two different metals.

to as electroforming. In this regard, Rand et al. have detected oxidized gold migration by TOF-SIMS using depth profiles when the device is polarized at 0.8 V for 4 h.[27]

2.3. Introduction of Oxidized Metal in the Contact

As observed previously, when reactive metals are used the inductive response is masked by the large capacitive currents of the interfacial electrochemical reactions. For this reason, we next aim to understand if the introduction of oxidized Ag (I) that contains a positive charge allows the direct generation of conductive filaments and avoids the electrochemical reaction at positive voltages. This experiment should not generate additional halide vacancies due to the electrochemical reaction and migration of Ag$^+$ should be the main responsible for the activation of the memristor.

Devices were fabricated with AgI contact and the I–V characterization is shown in **Figure 4**a,b. As expected, the I–V response also depends on the scan rate as in all cases studied in this work. At high scan rates of 1 V s^{-1} the trace resembles very much that of Ag (0) (Figure 3d) but the capacitive peak is not observed at positive bias since silver is already oxidized. Alternatively, at low scan rates of 0.01 V s^{-1} a well-defined inductive response is observed without the interference of a capacitive peak. Importantly, very low threshold (V$_{th}$) voltages close to ≈0.2 V are obtained indicating that as the charged Ag$^+$ is already available it is ready to directly follow the electric field to form conductive filaments. Note that the system shows the expected capacitive peaks at negative voltages since Ag (I) can be reduced to Ag (0). Likewise, at intermediate scan rates of 0.1 V s^{-1} the V$_{th}$ is ≈0.2 V and the inductive response is stable. Overall, the current experiment suggests that in the presence of activated/oxidized metal ions, conductive metal filamentary formation is the main activation/deactivation
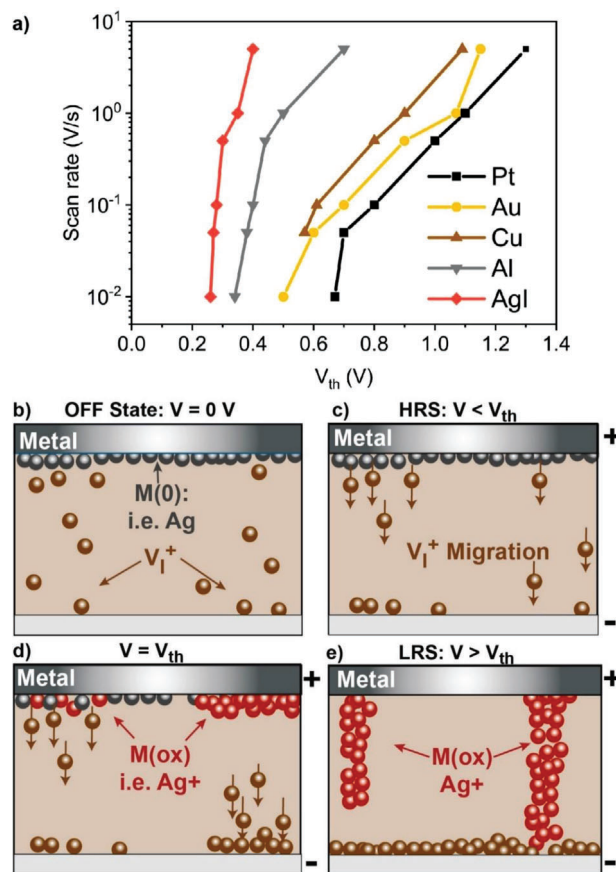
**ADVANCED
SCIENCE NEWS**
www.advancedsciencenews.com

**ADVANCED
FUNCTIONAL
MATERIALS**
www.afm-journal.de

Figure 4. a) Current–voltage (*I–V*) sweeps of devices fabricated in the configuration FTO/PEDOT:PSS/MAPbI$_3$/AgI/Au devices for 1 and 0.01 V s^{-1}, b) show 100 cycles at a scan rate of 0.1 V s^{-1}.

Figure 5. a) Summary of V_{th} of the different systems extracted from the *I–V* measured at different scan rates. Ag is not included due to the masking effect of the capacitive peak. b–e) Diagram showing the proposed activation mechanism.

mechanism in this type of memory devices. In addition, when activated Ag$^+$ ions are introduced in the system, and activation of the memristor occurs within the lowest V_{th} conditions reported for halide perovskites.

In the supplementary material, we show promising retention and cycling measurements for neuromorphic computing applications that require volatile memories with response time in the order of seconds and stable ON/OFF states for >2000 cycles. The use of AgI as an interfacial layer between the perovskite and the contact seems a very promising material for further development not only in model systems like those used in this work. Further performance improvement is expected using AgI in combination with buffer layers.

2.4. Dependence of Activation Voltage with the Metals and Proposed Overall Mechanism

Figure 5a shows the activation voltages (V_{th}) for the different metals extracted from the *I–V* curves at different scan rates. As can be observed, the V_{th} is minimum when active metal ions (Ag$^+$) are deliberately introduced in the system in the form of AgI. The V_{th} increases when a neutral metal (0) is introduced during de-

vice fabrication. The V_{th} of metals (0) follows a trend connected to their relative reactivity in which the most reactive metals (i.e., Al) show the lowest V_{th} and the least reactive metals (Au or Pt) show the highest V_{th}. In other words, it appears that formation of oxidized metals is needed to form the conductive filaments. This could be caused either by the direct migration of the charged metals or by an increase in the halide vacancies concentration generated by this electrochemical reaction, in both cases leading to the formation of conductive filaments. In any case, it is clear that the metal first needs to be electrochemically oxidized to be able to follow the applied electric field. Moreover, it appears that in the presence of oxidized metal ions, the effect of the metal is more important than the effect of the halide vacancies as it leads to a reduction of the V_{th}.

In order to verify the inductive and capacitive processes, Impedance Spectra (IS) has been carried out for devices with a nearly inert metal (Au) and pre-oxidized metal (AgI) (see Supporting Information). The inductive process appears at lower voltages (≈0.2 V) in devices with pre-oxidized metal (AgI) and at higher voltages (≈0.4 V) in devices with less reactive metals (Au), indicating a good agreement between results shown in Figure 5a and impedance spectra.

It is important to highlight that the capacitive process takes place at lower voltages than the inductive effect since the memory response requires the presence of oxidized metals. This is observed in both the I–V curves and by Impedance Spectroscopy (IS) measurements, shown in the supplementary information. For example, Figure 2e shows a device containing Au initially measured sweeping the voltage from 0 V toward positive bias. Under these conditions, the external voltage promotes halide vacancies and oxidized metal particles to move toward one of the contacts leading to charged external interfaces. In this manner, a capacitor will be formed with a typical double-layer capacitance in the order of ≈ 10 μFcm^2, these values are clearly supported by IS for the device containing Au (Figure S5, Supporting Information) at frequencies below 1 Hz at $V = 0$ V. At the threshold voltage of 0.5 V in Figure 2e, the oxidation of the metal occurs, and the inductive behavior is observed in the I–V curve. Similarly, Impedance spectroscopy data agrees with the I–V curve showing an inductive loop at voltages above ≈ 0.5 V (Figure S5, Supporting Information).

The capacitive current is maximized and becomes dominant with reactive metals, see Figure 3f, since there is a favored electrochemical reaction occurring. The inductive feature is masked and can only be observed when most of the Ag is already oxidized at voltages $V > 1.0$ V. Alternatively, when AgI is used, the formation of the inductive response is shifted to lower voltages in both I–V curve and IS data because the redox reaction is not needed since Ag is pre-oxidized.

The proposed activation mechanism is shown in Figure 5b–e. When the device is in the OFF state in the absence of an electric field ($V = 0$ V) the perovskite material contains a background concentration of halide vacancies and the metal contact is mostly in the metallic form, M (0). As a positive voltage is applied ($V < V_{th}$) halide vacancies migrate to the negative contact (Figure 5c). At the threshold voltage ($V = V_{th}$) the metal top contact begins to oxidize and most of the halide vacancies are close to the negative contact (Figure 5d). Finally, at applied voltages beyond the threshold voltage ($V > V_{th}$) metal ions begin to oxidize and migrate toward the negative contact increasing the conductivity of the perovskite material. The opposite processes would occur once the voltage is reversed.

Here it is important to note that the presence of AgI does not seem to be responsible for the increase in conductivity since the electrical conductivity of AgI[28] is on the same order of magnitude ($\approx 10^{-7}$ S cm^{-1}) to that of the MAPbI$_3$.[29] Alternatively, silver metal has been widely used in the literature to enhance the electrical conductivity of semiconductors. For example, Ag has been used as dopant in metal oxides such as ZnO or TiO$_2$ enhancing their conductivity by several orders of magnitude from 10^{-3}–10^{-4} to 10^1 S cm^{-1}. This approach has also been applied to other perovskite materials. In most cases, silver is present in the oxidized form when it is used as a dopant to increase the electrical conductivity of a material. When silver atoms are introduced into a material, they typically donate their valence electrons to the host material, which results in the formation of Ag$^+$ ions that are embedded within the host material. For example, in the case of silver-doped zinc oxide (Ag-doped ZnO), the silver atoms donate electrons to the ZnO lattice, leading to the formation of Ag$^+$ ions that are distributed throughout the ZnO crystal. These Ag$^+$ ions act as electron donors and enhance the electrical conductivity of the ZnO material.[30,31] Therefore, here we propose that the oxidized metals act as dopant that increase the bulk conductivity of the halide perovskite material.

Overall, we believe that the conductivity massively increases due to the insertion of migrating ions into the perovskite material leading to formation of percolation pathways. The modification of the energy barriers at the external interfaces due to the presence of ions is also important, in the extreme cases leading to electrochemical reactions. However, it is also possible that other effects such as the electrical field screening due to the presence of the charged ions will play a role, however, in any case, it seems to be a minor effect in the current device configuration.

3. Conclusion

In conclusion, we have shown that formation of oxidized metal ions (M$^+$) is required to provide the memory response, and the threshold voltage correlates with the reactivity of the contact., i.e., low reactivity contacts require high applied voltage that oxidizes the metal and SETs the low resistive state of the memristor. Activation could proceed either by the direct migration of the charged metals or by an increase in the concentration of halide vacancies generated by this electrochemical reaction, in both cases conductive filaments would be formed. In addition, the use of pre-oxidized Ag$^+$ ions introduced by deposition of a silver iodide layer leads to very low V_{th} (≈ 0.2 V) indicating that silver filamentary formation is very efficient at activating the memristor. The use of AgI as an interfacial layer is presented as very promising for low-energy applications and further work is expected in combination with buffer layers.

Supporting Information

Supporting Information is available from the Wiley Online Library or from the author.

Conflict of Interest

The authors declare no conflict of interest.

Data Availability Statement

The data that support the findings of this study are available from the corresponding author upon reasonable request.

[1] H. Kim, J. S. Han, S. G. Kim, S. Y. Kim, H. W. Jang, *J. Mater. Chem. C* **2019**, *7*, 5226.

[2] M. Y. Liao, Y. C. Chiang, C. H. Chen, W. C. Chen, C. C Chueh, *ACS Appl. Mater. Interfaces* **2020**, *12*, 36398.

[3] I. Chao, Y. T. Yang, M. H. Yu, C. H. Chen, C. H. Liao, B. H. Lin, I. Ni, W. C. Chen, A. W. Y. Ho-Baillie, C. C. Chueh, *Small* **2023**, *19*, 2207734.

[4] a) W. Xu, H. Cho, Y.-H. Kim, Y.-T. Kim, C. Wolf, C.-G. Park, T.-W. Lee, *Adv. Mater.* **2016**, *28*, 5916; b) Z. Xiao, J. Huang, *Adv. Electron. Mater.* **2016**, *2*, 1600100.

[5] a) J. Choi, J. S. Han, K. Hong, S. Y. Kim, H. W. Jang, *Adv. Mater.* **2018**, *30*, 1704002; b) R. A. John, N. Yantara, S. E. Ng, M. I. B. Patdillah, M. R. Kulkarni, N. F. Jamaludin, J. Basu, Ankit, S. G. Mhaisalkar, A. Basu, N. Mathews, *Adv. Mater.* **2021**, *33*, 2007851; c) J.-Q. Yang, R. Wang, Z.-P. Wang, Q.-Y. Ma, J.-Y. Mao, Y. Ren, X. Yang, Y. Zhou, S.-T. Han, *Nano Energy* **2020**, *74*, 104828.

[6] a) X. Yang, Z. Xiong, Y. Chen, Y. Ren, L. Zhou, H. Li, Y. Zhou, F. Pan, S.-T. Han, *Nano Energy* **2020**, *78*, 105246; b) M. S. Kim, M. S. Kim, G. J. Lee, S.-H. Sunwoo, S. Chang, Y. M. Song, D.-H. Kim, *Adv. Mater. Technol.* **2021**, 2100144.

[7] a) *Organic–Inorganic Halide Perovskite Photovoltaics: From Fundamentals to Device Architectures*, (Eds: N.-G. Park, M. Grätzel, T. Miyasaka), Springer, New York **2016**; b) J. Y. Kim, J.-W. Lee, H. S. Jung, H. Shin, N.-G. Park, *Chem. Rev.* **2020**, *120*, 7867.

[8] a) P. C. Harikesh, B. Febriansyah, R. A. John, N. Mathews, *MRS Bull.* **2020**, *45*, 641; b) Y. Park, J.-s. Lee, *J. Phys. Chem. Lett.* **2022**, *13*, 5638; c) X. Xiao, J. Hu, S. Tang, K. Yan, B. Gao, H. Chen, D. Zou, *Adv. Mater. Technol.* **2020**, *5*, 1900914.

[9] C. Eames, J. M. Frost, P. R. F. Barnes, B. C. O'Regan, A. Walsh, M. S. Islam, *Nat. Commun.* **2015**, *6*, 2.

[10] a) J. Bisquert, A. Guerrero, C. Gonzales, *ACS Phys. Chem. Au* **2021**, *1*, 25; b) O. Almora, C. Aranda, I. Zarazua, A. Guerrero, G. Garcia-Belmonte, *ACS Energy Lett.* **2016**, *1*, 209; c) W. Tress, J. P. Correa Baena, M. Saliba, A. Abate, M. Graetzel, *Adv. Energy Mater.* **2016**, *6*, 1600396; d) F. Wu, R. Pathak, K. Chen, G. Wang, B. Bahrami, W.-H. Zhang, Q. Qiao, *ACS Energy Lett.* **2018**, *3*, 2457.

[11] a) H. J. Gogoi, K. Bajpai, A. T. Mallajosyula, A. Solanki, *J. Phys. Chem. Lett.* **2021**, *12*, 8798; b) X. Zhao, H. Xu, Z. Wang, Y. Lin, Y. Liu, *InfoMat* **2019**, *1*, 407; c) Y. Fang, S. Zhai, L. Chu, J. Zhong, *ACS Appl. Mater. Interfaces* **2021**, *13*, 17141.

[12] M. Lanza, H. S. P. Wong, E. Pop, D. Ielmini, D. Strukov, B. C. Regan, L. Larcher, M. A. Villena, J. J. Yang, L. Goux, A. Belmonte, Y. Yang, F. M. Puglisi, J. Kang, B. Magyari-Köpe, E. Yalon, A. Kenyon, M. Buckwell, A. Mehonic, A. Shluger, H. Li, T. H. Hou, B. Hudec, D. Akinwande, R. Ge, S. Ambrogio, J. B. Roldan, E. Miranda, J. Suñé, K. L. Pey, et al., *Adv. Electron. Mater.* **2019**, *5*, 1800143.

[13] a) K. J. Kwak, D. E. Lee, S. J. Kim, H. W. Jang, *J. Phys. Chem. Lett.* **2021**, *12*, 8999; b) K. Kang, K. Hu, X. Tang, *J. Phys. Chem. Lett.* **2021**, *12*, 11673; c) Y. V. Pershin, M. Di Ventra, *Adv. Phys.* **2011**, *60*, 145; d) M. Rahimi Azghadi, Y.-C. Chen, J. K. Eshraghian, J. Chen, C.-Y. Lin, A. Amirsoleimani, A. Mehonic, A. J. Kenyon, B. Fowler, J. C. Lee, Y.-F. Chang, *Adv. Intell. Syst.* **2020**, *2*, 1900189; e) J. Bisquert, A. Guerrero, *J. Am. Chem. Soc.* **2022**, *144*, 5996.

[14] A. Solanki, A. Guerrero, Q. Zhang, J. Bisquert, T. C. Sum, *J. Phys. Chem. Lett.* **2020**, *11*, 463.

[15] a) C. Gonzales, A. Guerrero, J. Bisquert, *Appl. Phys. Lett.* **2021**, *118*, 073501; b) C. Gonzales, A. Guerrero, *J. Phys. Chem. Lett.* **2023**, *14*, 1395.

[16] X. Xiao, J. Hu, S. Tang, K. Yan, B. Gao, H. Chen, D. Zou, *Adv. Mater. Technol.* **2020**, *5*, 1900914.

[17] a) R. A. John, Y. Demirağ, Y. Shynkarenko, Y. Berezovska, N. Ohannessian, M. Payvand, P. Zeng, M. I. Bodnarchuk, F. Krumeich, G. Kara, I. Shorubalko, M. V. Nair, G. A. Cooke, T. Lippert, G. Indiveri, M. V. Kovalenko, *Nat. Commun.* **2022**, *13*, 2074; b) R. A. John, N. Shah, S. K. Vishwanath, S. E. Ng, B. Febriansyah, M. Jagadeeswararao, C. H. Chang, A. Basu, N. Mathews, *Nat. Commun.* **2021**, *12*, 3681; c) B. Ku, B. Koo, A. Sergeevich, M. Jae, C. Choi, *J. Alloys Compd.* **2020**, *833*, 155064.

[18] S. Satapathi, K. Raj, Yukta, M. A. Afroz, *Phys. Rev. Appl.* **2022**, *18*, 017001.

[19] a) J. M. Azpiroz, E. Mosconi, J. Bisquert, F. De Angelis, *Energy Environ. Sci.* **2015**, *8*, 2118; b) A. Senocrate, J. Maier, *J. Am. Chem. Soc.* **2019**, *141*, 8382; c) H. Wang, A. Guerrero, A. Bou, A. M. Al-Mayouf, J. Bisquert, *Energy Environ. Sci.* **2019**, *12*, 2054; d) K. Domanski, J.-P. Correa-Baena, N. Mine, M. K. Nazeeruddin, A. Abate, M. Saliba, W. Tress, A. Hagfeldt, M. Grätzel, *ACS Nano* **2016**, *10*, 6306.

[20] a) A. Guerrero, J. You, C. Aranda, Y. S. Kang, G. Garcia-Belmonte, H. Zhou, J. Bisquert, Y. Yang, *ACS Nano* **2016**, *10*, 218; b) M. Jeong, I. W. Choi, E. M. Go, Y. Cho, M. Kim, B. Lee, S. Jeong, Y. Jo, H. W. Choi, J. Lee, J.-H. Bae, S. K. Kwak, D. S. Kim, C. Yang, **2020**, *369*, 1615; c) H. Min, D. Y. Lee, J. Kim, G. Kim, K. S. Lee, J. Kim, M. J. Paik, Y. K. Kim, K. S. Kim, M. G. Kim, T. J. Shin, S. Il Seok, *Nature* **2021**, *598*, 444.

[21] M. Berruet, J. C. Pérez-Martínez, B. Romero, C. Gonzales, A. M. Al-Mayouf, A. Guerrero, J. Bisquert, *ACS Energy Lett.* **2022**, *7*, 1214.

[22] L. M. Díaz, A. J. Rosa, A. Bou, R. S. Sánchez, B. Romero, R. A. John, M. V. Kovalenko, A. Guerrero, *J. Bisquert, Front. Energy Res. 10*, **2022**, 914115.

[23] C. Gu, J.-S. Lee, *ACS Nano* **2016**, *10*, 5413.

[24] J. Pospisil, A. Guerrero, O. Zmeskal, M. Weiter, J. J. Gallardo, J. Navas, G. Garcia-Belmonte, *Adv. Funct. Mater.* **2019**, *0*, 1900881.

[25] Y. Kato, L. K. Ono, M. V. Lee, S. Wang, S. R. Raga, Y. Qi, *Adv. Mater. Interfaces* **2015**, *2*, 1500195.

[26] C. Gonzales, A. Guerrero, J. Bisquert, *J. Phys. Chem. C* **2022**, *126*, 13560.

[27] R. A. Kerner, L. Zhao, S. P. Harvey, J. J. Berry, J. Schwartz, B. P. Rand, *ACS Energy Lett.* **2020**, *5*, 3352.

[28] J. F. Jurado, J. A. Trujillo, B. E. Mellander, R. A. Vargas, *Solid State Ionics* **2003**, *156*, 103.

[29] N. Leupold, A. L. Seibel, R. Moos, F. Panzer, *Eur. J. Inorg. Chem.* **2021**, *2021*, 2882.

[30] F. Xian, K. Miao, X. Bai, Y. Ji, F. Chen, X. Li, *Optik* **2013**, *124*, 4876.

[31] M. Lanjewar, J. V. Gohel, *Inorg. Nano-Met. Chem.* **2017**, *47*, 1090.